# Real-time feedback control of flow-induced cavity tones. Part 1: fixed-gain control

M.A. Kegerise [a,*], R.H. Cabell [b] L.N. Cattafesta, III [c]

[a] *NASA-Langley Research Center, Flow Physics and Control Branch, Mail Stop 170, Hampton, VA 23681*

[b] *NASA-Langley Research Center, Structural Acoustics Branch, Mail Stop 463, Hampton, VA 23681*

[c] *University of Florida, Mechanical and Aerospace Engineering, P.O. Box 116250, Gainesville, FL 32611*

## Abstract

A generalized predictive control (GPC) algorithm was formulated and applied to the cavity flow-tone problem. The control algorithm demonstrated multiple Rossiter-mode suppression at fixed Mach numbers ranging from 0.275 to 0.38. Controller performance was evaluated with a measure of output disturbance rejection and an input sensitivity transfer function. The results suggest that disturbances entering the cavity flow are collocated with the control input at the cavity leading edge. In that case, only tonal components of the cavity wall-pressure fluctuations can be suppressed and arbitrary broadband pressure reduction is not possible with the present sensor/actuator arrangement. In the control-algorithm development, the cavity dynamics were treated as linear and time invariant (LTI) for a fixed Mach number. The experimental results lend support to that treatment.

*Key words:* cavity flow, cavity resonance, flow control, active flow control, generalized predictive control
*PACS:*

## 1 Introduction

The grazing flow over a cavity is characterized by an aeroacoustic feedback process that leads to large-amplitude acoustic tones. This cavity flow-tone

---

* Corresponding author.
  *Email address:* `michael.a.kegerise@nasa.gov` (M.A. Kegerise).

generation is of practical concern to several engineering applications ranging from weapons bays and landing gear in aircraft to flow over ground vehicles. In particular, the high sound pressure levels ($\sim$ 160 dB) associated with weapons bay tones can be damaging to stores within the bay and can influence the trajectory of released stores [1]. The physics of cavity flows has been the source of considerable study over the past four decades, and several review articles on the problem are available in the literature [2–4]. The salient features of the cavity-tone process are illustrated in Fig. 1 and are described as follows. Instability waves in the turbulent free shear layer spanning the cavity grow and convect downstream. The resulting unsteady impingement on the downstream corner acts as a noise source. Sound from this source propagates upstream to the cavity leading edge. Here, the feedback disturbances are converted to instability waves through a receptivity process to complete the feedback loop. Power spectra of unsteady pressures within the cavity often exhibit multiple narrowband tones that result from the aeroacoustic feedback process described above. These peaks are referred to a "Rossiter modes" after the author who first studied the phenomenon [5].

Previous studies aimed at the suppression of cavity-flow tones have employed passive and open-loop active flow-control methodologies. Feedback flow control, however, has only recently been applied to the problem [6–12]. An overview of various feedback-control methodologies is given in the review paper by Cattafesta *et al.* [13]. There are particular benefits to this approach over passive or open-loop control methods, such as reduced energy consumption [10], no drag penalty, and robustness to parameter changes and modeling uncertainties. For example, a feedback control algorithm can be made to adapt to changes in process dynamics that are brought about by changes in freestream conditions.

Aside from the practical interest, the cavity-flow problem is an excellent test bed for real-time, closed-loop flow control. Here, real-time implies that the control effort is computed at the sample rate of a digital controller. Although the geometry is relatively simple and only a small number of narrowband tones are to be suppressed, the physics of the process is both rich and complex. Specifically, the multiple Rossiter modes often experience significant nonlinear coupling and mode switching [14–16], the dynamics of the process are sensitive to freestream Mach number, and there are convective delays between control inputs and sensor outputs. These physical elements are present in many other active flow-control problems. It is expected therefore that control algorithms and approaches developed for this problem will find broader application. Most importantly, the required sensors, actuators, and digital signal processing (DSP) hardware are mature enough to enable real-time feedback control of flow-induced cavity tones.

The ultimate goal of the present research is self-tuning adaptive control of

cavity tones. Adaptive control, in particular, is necessary for this problem since the cavity-flow dynamics change as the freestream Mach number changes. The elements of a self-tuning adaptive controller are shown in Fig. 2. There are two distinct loops in this controller. The inner loop is a dynamic feedback control system comprised of the process and controller. In this loop, the controller operates at a sample rate that is suitable for the process under control. The output of the process is unsteady pressures at the cavity walls. The reference signal is set to zero since the control objective is to minimize the output. The outer loop consists of the model estimation and controller design steps. Model estimation refers to the identification of a model from process input-output data. The identified process parameters and a specified cost function are then used to design a controller that will minimize the output pressures. In a fully adaptive controller, both steps are performed recursively at the sample rate of the controller; *i.e.*, in real time. If the process dynamics vary slowly, however, the parameter identification and controller update can be performed at a slower rate or possibly offline in a batch mode.

This article is the first of two parts that describe experiments aimed at the development of a real-time adaptive controller for the cavity flow-tone problem. As a first step to that end, the model identification and controller design steps were performed offline in a batch mode. The cavity dynamics were assumed to be linear and time invariant for any given *fixed* Mach number. The result was a series of linear, fixed-gain control laws valid only for the freestream Mach numbers at which they were designed. These control laws were then applied to a cavity-flow test bed. Limitations in the control performance were identified and the suitability of the linearity and time-invariance assumptions was examined. The key purpose of this first step was to identify whether the control methodology is sound, as it is the basis for a recursive controller design algorithm.

The article is organized as follows. The control methodology and algorithm are presented in the next section. This is followed by a description of the experimental setup and data processing methods. Next, the primary characteristics of the baseline cavity flow are presented. The results of the control experiments are then presented and discussed. Finally, limitations in the control performance are identified and discussed.

## 2   Control Methodology

In the feedback control of cavity-flow tones, the objective is to minimize the output fluctuating pressure on the cavity walls. This is a disturbance rejection problem in controls terminology. The output pressures are provided by a discrete number of transducers embedded in the cavity walls. These signals

serve as both feedback signals and as performance measures for the controller. To achieve the control objective, actuation is applied at the cavity leading edge with the aim to cancel shear layer instability waves that result from the aeroacoustic feedback loop. This effectively breaks the feedback loop, and results in a global reduction in the cavity-tone amplitudes. Cattafesta *et al.* [10] and Williams *et al.* [6,7] previously demonstrated the potential for this control approach to suppress cavity tones.

Actuation at the cavity leading edge is particularly advantageous since the flow is most receptive at that point. Therefore, the required control-input amplitude and energy requirements will be minimized. In previous feedback control studies of cavity tones, two types of actuators were employed: mechanical vibration of the cavity leading edge with a flap actuator [10,12] and zero-net mass flux actuation through a spanwise slot at the leading edge [6,7,9]. The two-dimensional nature of these input types is compatible with the character of the instability waves being targeted for suppression. A piezoelectric flap-type actuator was used in the current study.

## 2.1  System Identification

In many control-design approaches, a mathematical model of the process must be available for controller design. While a physics-based model is desirable, none of sufficient accuracy is currently available. Instead, an empirical model, whose parameters are determined from input-output data, can be used. Calculation of the parameters is referred to as system identification.

Recently, Rowley *et al.* [31,32] suggested that cavity oscillations can be characterized as either self-sustained or forced. In the self-sustained regime, the cavity flow is linearly unstable with tone amplitudes limited by nonlinear saturation of instabilities in the cavity shear layer. In the forced regime, the oscillations result from the amplification of external disturbances (*e.g.*, turbulent boundary-layer fluctuations). In effect, the cavity flow behaves as a linearly stable, lightly-damped system that amplifies disturbances at certain resonant frequencies. The character of the oscillations dictates the experimental approach to identifying the model parameters. For example, if they are self-sustained, the system must be stabilized prior to data collection for system identification. That approach was used by Williams *et al.* [33] and Rowley *et al.* [31] to identify and control a cavity flow in the self-sustained regime. Otherwise, system identification can be used to identify the parameters for a model of the open loop cavity dynamics.

It will be shown in the results section that the cavity-flow oscillations for the present study can be characterized as the forced response of a lightly-damped

4

system. Therefore, the model structure chosen to represent the open loop cavity-flow dynamics was a discrete-time linear model given by:

$$y(k) = \alpha_1 y(k-1) + \ldots + \alpha_p y(k-p) + \beta_0 u(k) + \ldots + \beta_p u(k-p), \quad (1)$$

where $y(k)$ are the $m \times 1$ outputs, $u(k)$ are the $r \times 1$ inputs, $p$ is the model order, and $k$ is the current time step. This model structure is commonly referred to as an ARX (auto-regressive, exogenous input) model [18,19]. The coefficient matrices, $\alpha_i$ $(i = 1, 2, \ldots, p)$ of $m \times m$ and $\beta_i$ $(i = 0, 1, 2, \ldots, p)$ of $m \times r$, are the ARX parameters or the observer Markov parameters.

To determine the observer Markov parameters of the model, the observer/Kalman filter identification (OKID) algorithm of Juang *et al.* [18,21,22] was used. The OKID algorithm identifies plant parameters from experimental input-output data from the open-loop plant. To obtain this data, the actuator was driven with a broadband signal and input-output time-series data were collected. Models were identified for each of the flow conditions considered in the control experiments.

## 2.2   *Generalized Predictive Control (GPC)*

There are several control-design methods that can be used to meet the present control objective. The particular control law used in this study was the generalized predictive controller (GPC). The GPC algorithm is based on system output predictions over a finite time horizon. Using these predictions, an appropriate cost function for the problem is then defined and subsequently minimized to determine the control law. The GPC was first introduced by Clarke *et al.* [23,24] and has since been successfully applied to many active vibration and noise control problems. It is applicable to plants that are non-minimum phase, plants that are open-loop unstable or have lightly-damped poles, and plants that have delays. Since the cavity-flow dynamics exhibit several of these features, the GPC was considered to be a good candidate for the problem.

A predictive matrix equation that provides future system output predictions can be formed from the ARX model in Eq. 1 [21,22,25,26]:

$$\mathbf{y}_s(k) = \mathbf{T}\mathbf{u}_s(k) + \mathbf{\Theta}\mathbf{v}_p(k-p), \quad (2)$$

where $\mathbf{y}_s(k)$ is an $sm \times 1$ vector of current and future outputs:

$$\mathbf{y}_s(k) = \left\{ \begin{array}{c} y(k) \\ y(k+1) \\ \vdots \\ y(k+s-1) \end{array} \right\}, \tag{3}$$

$\mathbf{u}_s(k)$ is an $sr \times 1$ vector of current and future inputs:

$$\mathbf{u}_s(k) = \left\{ \begin{array}{c} u(k) \\ u(k+1) \\ \vdots \\ u(k+s-1) \end{array} \right\}, \tag{4}$$

and $\mathbf{v}_p(k-p)$ is a $p(m+r) \times 1$ vector of past inputs and outputs running from time step $k-p$ to $k-1$:

$$\mathbf{v}_p(k-p) = \left\{ \begin{array}{c} u(k-p) \\ \vdots \\ u(k-1) \\ y(k-p) \\ \vdots \\ y(k-1) \end{array} \right\}. \tag{5}$$

The parameter $s$ is referred to as the prediction horizon. The predictive matrix equation states that the future output data depends on the future control inputs and past input-output data. The matrix $\mathbf{T}$ is an $sm \times sr$ Toeplitz matrix:

$$\mathbf{T} = \left[ \begin{array}{ccccc} \beta_0 & & & & \\ \beta_0^{(1)} & \beta_0 & & & \\ \beta_0^{(2)} & \beta_0^{(1)} & \beta_0 & & \\ \vdots & \vdots & \ddots & \ddots & \\ \beta_0^{(s-1)} & \beta_0^{(s-2)} & \cdots & \beta_0^{(1)} & \beta_0 \end{array} \right] \tag{6}$$

6

where $\beta_0$, $\beta_0^{(1)}$, $\cdots$, $\beta_0^{(s-1)}$ are the pulse response parameters of the open loop plant. These parameters can be obtained from the observer Markov parameters [21]. The rectangular matrix $\Theta$ is formed with a set of recursive equations and the ARX parameters [21].

Since the present control objective is disturbance rejection at the system output, the appropriate cost function for the GPC algorithm is given by:

$$J = \mathbf{y}_s^T(k)\mathbf{Q}\mathbf{y}_s(k) + \mathbf{u}_s^T(k)\lambda\mathbf{u}_s(k). \tag{7}$$

The first term in Eq. 7 is the sum of the weighted, squared output values over the prediction horizon and $\mathbf{Q}$ is an $sm \times sm$ block-diagonal matrix of sensor weights:

$$\mathbf{Q} = \begin{bmatrix} Q_1 & 0 & 0 \\ 0 & \ddots & 0 \\ 0 & 0 & Q_s \end{bmatrix} \tag{8}$$

where $Q_i$ is an $m \times m$ diagonal matrix of sensor weights:

$$Q_i = diag\left(q_1, q_2, \cdots, q_m\right). \tag{9}$$

The sensor weights $q_1, \cdots, q_m$ take on values between 0 and 1. A value of zero means that the sensor is not included in the cost function, but the sensor information will still be used by the feedback controller. The second term in the cost function imposes an effort penalty on the control inputs and $\lambda$ is a positive scalar value. This term is necessary to avoid large control inputs and actuator saturation. It also affects the closed loop system stability.

To determine the control law, the cost function is minimized with respect to the control input. Substituting Eq. 2 into Eq. 7 and minimizing the result with respect to $\mathbf{u}_s$ gives:

$$\mathbf{u}_s(k) = -\left[\mathbf{T}^T\mathbf{Q}\mathbf{T} + \lambda\mathbf{I}\right]^{-1}\mathbf{T}^T\mathbf{Q}\Theta\mathbf{v}_p(k-p), \tag{10}$$

where $\mathbf{I}$ is an $sr \times sr$ identity matrix. This control law yields a vector of current and future control inputs. In the real-time implementation of this control law, however, the current control effort, $u(k)$, is applied to the system and the future values are discarded at each time step. Therefore, it is sufficient to compute the current control input as:

$$u(k) = \left\{-\left[\mathbf{T}^T\mathbf{Q}\mathbf{T} + \lambda\mathbf{I}\right]^{-1}\mathbf{T}^T\mathbf{Q}\right\}_r \Theta\mathbf{v}_p(k-p), \tag{11}$$

where the subscript $r$ denotes the first $r$ rows of the matrix in brackets. Recall that the cavity dynamics are assumed to be time invariant for a given *fixed* Mach number. The matrix premultiplying $\mathbf{v}_p(k-p)$ in Eq. 11 can then be evaluated offline using the identified ARX parameters for each of the test Mach numbers. With this approach, a series of fixed-gain control laws, valid only for the Mach numbers at which they were designed, is obtained.

There are several parameters in the GPC algorithm that must be tuned to achieve a balance between optimal performance and stability of the controller: the model order $p$, the prediction horizon $s$, the control effort penalty $\lambda$, and the sampling rate. Although the parameter values are problem dependent, experience provides some guidelines for their selection. The model order is selected through system identification. The key issue in this case is to chose $p$ large enough such that all of the pertinent open-loop dynamics are captured by the model. The prediction horizon should be at least equal to the model order, but in practice, is typically taken as 2 to 3 times the model order [25]. The optimal value for the control effort penalty must be determined through on-line testing. Small values of $\lambda$ result in an aggressive controller while large values result in a more sluggish controller. If the system to be controlled is non-minimum phase, the controller will be unstable when $\lambda = 0$ [22]. For the sampling rate, experience indicates that a value 2 to 3 times the highest frequency results in the best performance [25].

## 3  Experimental Details

The experiments were conducted at NASA-Langley Research Center in the Probe Calibration Tunnel (PCT). The PCT is typically operated as an open-jet pressure tunnel with independent control over stagnation pressure, stagnation temperature, and freestream velocity. For the current experiments, the facility was fitted with a subsonic nozzle that contracts from a 304.8 mm circular inlet to a 50.8 mm by 152.4 mm exit. A straight duct section of length 0.6 m was attached to the nozzle exit and was terminated with a small-angle diffuser. The freestream Mach number range for the present tunnel configuration was 0.04 to 0.8.

A rectangular cavity model was installed in the ceiling of the straight duct section of the PCT. The floor of the duct section was a foam filled baffle that minimized reflections of acoustic waves radiated by the cavity. The cavity model had a fixed length, $\ell = 152.4$ mm, and a variable depth, $d$, that was fixed at 30.48 mm to give an $\ell/d$ ratio of 5. The cavity model spanned the width of the test section ($w = 50.89$ mm) to provide an un-obscured view of the cavity shear layer for optical diagnostics. The incoming boundary layer was turbulent with a thickness of $\delta \approx 6$ mm. A schematic of the cavity model

is shown in Fig. 3.

The cavity model was instrumented with a pair of piezoresistive pressure transducers. The nominal sensitivity and bandwidth of the sensors were $2.2 \times 10^{-5}$ V/Pa and 14 kHz, respectively. One sensor was located in the midplane of the front cavity wall, 12 mm down from the cavity leading edge. The second sensor was located in the floor midplane, 15 mm upstream from the cavity rear wall (see Fig. 3).

The actuator for the present study was a piezoelectric bimorph cantilever beam with its tip situated at the cavity leading edge (Fig. 3). In this orientation, the actuator tip moves normal to the main flow direction. This actuator was chosen for its relatively high bandwidth ($\sim$ 1 kHz) and ability to generate large streamwise disturbances with modest tip deflections (on the order of tens of micrometers [8,27]). The measured frequency response function of the actuator, from input voltage to output tip deflection, is shown in Fig. 4. As observed in the figure, the actuator response is characteristic of a 2nd-order under-damped system with a natural frequency of $\approx$ 1200 Hz and a DC gain of $\approx 0.25$ $\mu$m/V. Further details on the design and construction of the actuator can be found in Kegerise $et$ $al.$ [8], Mathew [28] and Schaeffler $et$ $al.$ [29]

Details of the hardware setup for the feedback control experiments are shown in Fig. 5. The voltage signals from the cavity pressure sensors were first pre-amplified and anti-alias filtered with 6th-order time delay filters. These filters were chosen for their constant group delay ($0.715/F_c$ seconds) in the passband. The cutoff frequency of the filters was set to $F_c = 1600$ Hz. Next, the signals were sampled with a 16-bit A/D.

The control algorithm was coded to run on a floating-point DSP with a clock speed of 480 MHz. Based on the current and past sampled voltages from the pressure sensors and past control efforts, the control algorithm computed the control signal once per time step. For all of the results presented in this article, the sample time of controller was set to 250 $\mu$s.

The computed control effort was converted to an analog signal via a 14-bit D/A card. This signal was passed to a reconstruction filter (same type as the anti-alias filter with $F_c = 1600$ $Hz$) to smooth the zero-order hold signal from the D/A card. The output of this filter was sent to a high-voltage amplifier to produce the drive signal for the bimorph actuator.

Pressure sensor time-series data were collected for both the baseline (open-loop) and the controlled cavity flow. Primarily, these data were processed to obtain pressure spectra. In computing the spectra, 1024 point FFTs, a hanning window, 50% overlap, and 160 block averages were used. The sample rate for data collection was 4 kHz and the frequency resolution of the spectra was 3.9 Hz. The pressure spectra are presented in the results section as dB re $2.0 \times 10^{-5}$

Pa.

## 4  Results and Discussion

### *4.1  Baseline Cavity Flow*

The baseline (control off, open loop) cavity flow was first evaluated. To that end, unsteady pressure time series were acquired for a range of freestream Mach numbers ($M_\infty = 0.1$ to 0.6). The total pressure and total temperature were held constant at 138 kPa and 297 K, respectively, during the acquisition. The spectra of the unsteady pressures were calculated and peaks in the pressure spectra that correspond to Rossiter modes were identified. The frequencies of these peaks were then compared to those obtained from the modified Rossiter equation [30]:

$$St_\infty = \frac{m - \alpha}{M_\infty \left(1 + \frac{\gamma - 1}{2} M_\infty^2\right)^{-1/2} + 1/\kappa}, \tag{12}$$

where $St_\infty = f\ell/U_\infty$ is the Strouhal number, $m\ (= 1, 2, 3, \ldots)$ is the mode number, and $\alpha = 0.25$ and $\kappa = 0.66$ are empirical constants. The measured and calculated Rossiter-mode frequencies for $m = 1$ to 5 are shown in Fig. 6. The agreement between the measured frequencies and those calculated via Eq. 12 was within 10%, verifying that the present cavity model behaves as expected.

Three test Mach numbers were chosen for feedback control: $M_\infty = 0.275, 0.32,$ and 0.38. The baseline pressure spectra of the rear-floor sensor for these Mach numbers is presented in Fig. 7. The characteristic multiple resonant tones that increase in frequency with increasing Mach number are evident. The tone amplitudes and broadband levels are also seen to increase with increasing Mach number. Note that all cavity tones for each case are within the bandwidth of the present actuator. Table 1 presents the measured and calculated frequencies of the first four Rossiter modes for each test condition. The good agreement between them (within 10%) establishes the quality of the testbed for feedback control experiments.

In the present control methodology, system identification is used to identify the parameters for a model of the open loop cavity-flow dynamics. As stated earlier, this approach is valid when the cavity oscillations can be characterized as forced, linearly stable. If the system was unstable, however, the cavity oscillations would have to be stabilized before performing system identification.

The probability density functions (PDF) of the cavity pressure signals can be used to determine which regime (forced, linearly stable or self-sustained, linearly unstable) characterizes the cavity oscillations [31]. For example, if the input disturbances have a Gaussian distribution, the PDF of a linearly stable system will also be Gaussian. The PDFs of the baseline rear-floor pressure for the three test Mach numbers are shown in Fig. 8. Within the uncertainty of the estimate, the PDFs of the pressures are observed to be Gaussian. The same statement applies to the pressures at the front-wall sensor. The cavity oscillations may therefore be characterized as forced, linearly stable, and system identification may be applied to the open-loop system.

*4.2 Control Results*

Using the identified models for the cavity dynamics, controllers were designed for each of the test Mach numbers using Eq. 11. These control laws were then implemented on the real-time DSP hardware. Initially, large values for the control effort penalty, $\lambda$, were used in control design and testing. Subsequent designs used progressively smaller values of $\lambda$ to move towards more aggressive controllers. Controller performance was evaluated through a comparison of the baseline and controlled wall-pressure spectra. The optimal value of $\lambda$ gave the best performance (*i.e.*, maximum tone suppression) while maintaining stability and avoiding actuator saturation.

The GPC algorithm parameters giving the best performance for the three test Mach numbers are shown in Table 2. For all cases, the model order used in system identification was 80 and the prediction horizon was set to 240 ($s = 3p$). The sensor weights for the two output sensors were zero for the front-wall sensor ($q_1$) and one for the rear-floor sensor ($q_2$). The control performance was found to be weakly dependent on the sensor weights, and only subtle differences were observed with different values of sensor weightings.

Figures 9a, 10a, and 11a present the baseline and controlled pressure spectra at the rear-floor sensor for the Mach numbers and control parameters listed in Table 2. Multiple Rossiter modes were suppressed by the control algorithm for all three conditions. For the $M_\infty = 0.275$ case in particular, the first four Rossiter modes exhibit some suppression. The dominant Rossiter mode, *i.e.*, the tone with maximum spectral amplitude, is suppressed by approximately 10 dB in each test case. The broadband levels of the pressure fluctuations are not significantly altered in any of the control runs. It is of interest to note that the same statements can be made in reference to the pressure spectra at the front-wall sensor. This implies that feedback control produces a global reduction in the cavity-tone amplitudes; a result that is expected in light of the present control approach.

### 4.2.1 Control Performance Limitations

In previous feedback control studies of cavity-flow tones, several performance limitations were noted. Specifically, the controllers excited new tones or side bands of the Rossiter modes [31,9]. The latter phenomenon is referred to as peak splitting. None of the previous studies reported significant reductions in the broadband pressure fluctuations. In the present control experiments, the excitation of new tones was not observed. While the pressure spectra do not indicate distinct peak splitting, a close examination of the controlled pressure spectra reveals increased energy in frequency bands around the Rossiter modes. This behavior, which is common in the feedback control of sound and vibration, is referred to as spillover. It follows from the definition of Hong and Bernstein [34] which states that spillover occurs at frequency $f$ when the closed-loop transfer-function magnitude is greater than the open-loop transfer function magnitude at that frequency. The result is disturbance amplification in the output sensors.

A performance measure can be defined to better represent the spillover observed in the control results:

$$\frac{\|\mathbf{y}_{cl}(f)\|_2}{\|\mathbf{y}_{ol}(f)\|_2}, \tag{13}$$

where $\mathbf{y}_{cl}$ and $\mathbf{y}_{ol}$ are vectors of the output sensor spectra for the controlled and baseline cases, respectively, and $\|\cdot\|_2$ is the 2-norm. Eq. 13 essentially provides a scalar measure of disturbance rejection for the multiple output sensors. A value less than one indicates disturbance attenuation, while a value greater then one indicates disturbance amplification. The performance measure was calculated for each of the control cases and the results are indicated by the dashed lines in Figs. 9b, 10b, and 11b. As expected, the performance measure is less than one (negative log magnitude) at the Rossiter modes where attenuation has occured, but this is always accompanied by amplification (positive log magnitude) in sideband frequencies.

To understand why spillover arises in the feedback control results, the definition of a sensitivity transfer function is useful. The sensitivity was recently used by Rowley *et al.* [31] to explain performance limitations in the feedback control of cavity tones. Towards that end, consider the single-input/multiple-output (SIMO) model for the cavity-flow control system shown in Fig. 12. The thicker lines indicate multidimensional signals, while the thinner lines indicate scalar signals. The disturbance, $w(t)$, is hypothesized to enter the system at the cavity leading edge, where the shear layer is especially receptive to inputs. The disturbance is subsequently filtered by the cavity dynamics before reaching the output sensors. In the absence of feedback control, this disturbance drives the response in the output sensors. This viewpoint is consistent

with the hypothesis that cavity-flow tones result from the forced response of a lightly-damped system.

The control input is hypothesized to follow the same path to the output sensors as the disturbance, as indicated in Fig. 12. With this hypothesis, anything the controller does to reject the disturbance will be reflected equally in all output sensors.

The input sensitivity for this SIMO system can be used to verify this hypothesis. The input sensitivity represents the transfer function between the disturbance, $w(t)$, and the plant input, $v(t)$, and is written as:

$$S_i = \frac{1}{1 - \mathbf{HP}},$$
(14)

where $\mathbf{P} = \mathbf{G}G_a$ is the plant transfer function and $\mathbf{H}$ is the controller transfer function. For a SIMO system with a single disturbance following the same path to the error sensors as the control input, the input sensitivity can be shown to be equal to the performance measure defined in Eq. 13. The mathematical details of this equality are presented in the appendix. If the disturbance follows another path or if there are multiple disturbance paths to the output sensors, then this will not be true.

The log magnitude of the input sensitivity $(20 \log (|S_i|))$ is indicated by the solid line in Figs. 9b, 10b, and 11b. The good agreement between the input sensitivity and the measured performance for the $M_\infty = 0.275$ case supports the above hypothesis that the disturbance enters the system at the input. As the Mach number is increased, however, the differences between them increase. These differences can arise from uncertainties in the plant model used to calculate $S_i$ and other disturbances that follow a different path to the output sensors. Nevertheless, for the Mach number range tested, the disturbance appears to follow the same path through the plant as the control input.

Recall that the input sensitivity was defined to aid in understanding the origins of spillover. Since the control objective is disturbance rejection, it is desired that $|S_i| < 1$ (negative log magnitude) over all frequencies. However, the Bode integral constraint places certain requirements on the sensitivity. Specifically, for a discrete data system with an asymptotically stable open-loop transfer function, $\mathbf{HP}$, the Bode integral constraint is [35]:

$$\int_0^\pi \log \left( \left| S_i \left( e^{j\omega} \right) \right| \right) d\omega = 0.$$
(15)

The immediate consequence of Eq. 15 is negative values of the log sensitivity in one frequency band must necessarily be balanced by positive values in

13

another frequency band. The result is spillover and the current performance data clearly reflect this integral constraint.

If spillover is unavoidable, then the best approach is to seek a control design the minimizes the input sensitivity at the cavity tone frequencies and balances this with $|S_i|$ slightly larger than one over a wide band of frequencies. There are, however, practical limits to approach. First, the actuators used in cavity control do not have sufficient authority over a wide frequency range. Second, the frequency band over which the sensitivity can be balanced is limited in a digital controller by the Nyquist frequency.

Instead, it is important to consider whether the constraints imposed by the Bode integral can be overcome and therefore achieve arbitrary levels of broadband pressure reduction. Hong and Bernstein [34] have shown that there are specific conditions under which a zero-spillover controller can be designed. One condition is that the disturbance and the control input be noncollocated. If they are collocated, then spillover is unavoidable. Since the present performance data suggest that the disturbance and control input are indeed collocated, spillover cannot be avoided. This is unfortunate since, from the standpoint of minimal control input energy, the cavity leading edge is an ideal place for actuation. From a controls perspective, however, it does not appear to be an optimal place to achieve *broadband* disturbance rejection.

### 4.2.2   Linearity and Time-Invariance Assumptions

In the control design, it was assumed that the cavity dynamics is linear and time invariant for a fixed Mach number. The PDF data presented earlier in this section lend support to the linear treatment. That data suggests that the overall cavity dynamics is characteristic of a forced, linearly-stable system; not limit cycle oscillations of an unstable system. Further support for the control-design assumptions is provided by the agreement between the measured control performance and the input sensitivity function that is based on a linear, time-invariant model of the cavity dynamics. Finally, the time-invariance of the cavity dynamics at a given Mach number was examined through repeated controller design and application over several hours of testing. For each Mach number considered in the tests, the controller yielded the same level of control performance.

If the Mach number varies, however, the assumption of time invariance no longer holds. To see this, consider the data plotted in Fig. 13. In the plot, the baseline pressure spectra of the rear-floor sensor at $M_\infty = 0.29$ is presented. Also plotted in the figure is a controlled pressure spectra of the rear-floor sensor at the same Mach number. That data was generated by applying the controller designed at $M_\infty = 0.275$ to the cavity flow at $M_\infty = 0.29$. Although the Mach

14

number has changed by only $\sim 9\%$ from the design condition, the cavity dynamics has changed enough to degrade the control performance, as indicated by the increased energy in Rossiter-mode sidebands. This underscores the need for an adaptive controller that can track changes in the system dynamics with varying Mach number. The development and application of an adaptive controller for the cavity problem will be presented in a companion article.

## 5   Conclusions

In this article, the real-time feedback control of cavity flow-tones was presented. Generalized predictive control laws were developed offline in a batch mode. A key assumption in this approach was that the cavity dynamics was linear and time invariant for any given *fixed* Mach number. The resulting series of linear fixed-gain control laws, valid only for the Mach numbers at which they were designed, was then applied to an experimental cavity flow test bed. The controllers achieved multiple Rossiter-mode suppression at fixed Mach numbers ranging from 0.275 to 0.38. Furthermore, the suppression is a global effect since all pressure sensors within the cavity experienced similar reductions in cavity-tone amplitudes.

Limitations in controller performance were examined through the use of an input sensitivity transfer function. The close agreement between the input sensitivity and a measure of output disturbance rejection suggests that the primary disturbance path is through the plant (cavity dynamics) from the input (cavity leading edge). This, in turn, suggests collocation of the control input and disturbance and therefore, arbitrary reduction of broadband unsteady cavity pressures is not possible with the present arrangement of sensors and actuator. Instead, spillover will occur at frequencies away from the Rossiter modes.

Alternative placements of actuators and sensors may overcome this performance limitation. One possible arrangement would utilize actuation at both the leading and trailing edges of the cavity. Measurements sensors in the cavity shear layer may also be useful since then, a disturbance signal that is time advanced from actuation at the trailing edge would be available. This feedforward type of arrangement may greatly enhance the control performance, particularly in regard to broadband disturbance rejection.

In the development of the GPC control laws, the cavity dynamics was treated as linear and time invariant (LTI) at a fixed Mach number. In view of the experimental control results, this appears to be a reasonable treatment of the problem. The control laws developed in this article, however, are valid only for the given Mach numbers at which they were designed. Small changes in Mach

number lead to changes in the cavity dynamics and that, in turn, leads to a degradation in control performance if a fixed-gain controller is used. Instead, the controller coefficients must be made to adapt to changing cavity dynamics. The control methodology presented in this article provides the framework for an adaptive controller. In the companion paper, an adaptive GPC algorithm is developed and the results of its application to the cavity flow test bed will be presented.

## 6 Appendix

In this section, the performance measure defined in Eq. 13 is shown to be equal to the input sensitivity for the SIMO model shown in Fig. 12. To that end, an expression for the closed-loop response of the SIMO system must first be formed. The cavity flow is considered to be a single-input/multiple-output system described by:

$$\mathbf{y}(f) = \mathbf{G}(f)v(f), \tag{16}$$

where $\mathbf{G}(f)$ is an $m \times 1$ frequency response function matrix of the cavity flow. The controller is a multiple-input/single-output system described by:

$$u(f) = \mathbf{H}(f)\mathbf{y}(f) \tag{17}$$

where $\mathbf{H}(f)$ is a $1 \times m$ frequency response function matrix of the controller. The input to the cavity flow is given by:

$$v(f) = w(f) + G_a(f)u(f). \tag{18}$$

Substituting Eqs. 17 and 18 into Eq. 16 yields:

$$\mathbf{y} = \mathbf{G}w + \mathbf{G}G_a\mathbf{H}\mathbf{y}, \tag{19}$$

where the dependence on frequency, $f$, is understood. Solving this expression for $\mathbf{y}$ gives the closed-loop response:

$$\mathbf{y} = [\mathbf{I} - \mathbf{G}G_a\mathbf{H}]^{-1}\mathbf{G}w. \tag{20}$$

Using the matrix inversion lemma:

$$[\mathbf{A} + \mathbf{BCD}]^{-1} = \mathbf{A}^{-1} - \mathbf{A}^{-1}\mathbf{B}\left[\mathbf{C}^{-1} + \mathbf{DA}^{-1}\mathbf{B}\right]^{-1}\mathbf{DA}^{-1}, \tag{21}$$

the matrix inverse in Eq. 20 can be written as:

$$\mathbf{I} + \mathbf{G} \left( \frac{1}{G_a} - \mathbf{HG} \right)^{-1} \mathbf{H} \tag{22}$$

or

$$\mathbf{I} + \frac{\mathbf{G}G_a\mathbf{H}}{1 - \mathbf{HG}G_a}. \tag{23}$$

Substituting this expression into Eq. 20 gives:

$$\mathbf{y} = \frac{\mathbf{G} - \mathbf{HG}G_a\mathbf{G} + \mathbf{G}G_a\mathbf{HG}}{1 - \mathbf{HG}G_a}w. \tag{24}$$

Since $\mathbf{HG}$ and $G_a$ are scalar transfer functions, Eq. 24 can be rewritten as:

$$\mathbf{y} = \frac{\mathbf{G} - \mathbf{G}G_a\mathbf{HG} + \mathbf{G}G_a\mathbf{HG}}{1 - \mathbf{HG}G_a}w \tag{25}$$

and therefore,

$$\mathbf{y} = \frac{\mathbf{G}}{1 - \mathbf{HG}G_a}w. \tag{26}$$

The input sensitivity for the SIMO system is given by:

$$S_i = \frac{1}{1 - \mathbf{HG}G_a} \tag{27}$$

Using this definition, the closed-loop response for the model system can be written as:

$$\mathbf{y}_{cl} = S_i\mathbf{G}w. \tag{28}$$

where the subscript was added to denote the closed-loop response.

In the absence of feedback control, the open-loop response of the cavity flow is described by:

$$\mathbf{y}_{ol} = \mathbf{G}w. \tag{29}$$

Recall the performance measure defined earlier:

$$\frac{\|\mathbf{y}_{cl}(f)\|_2}{\|\mathbf{y}_{ol}(f)\|_2} = \frac{\sqrt{\mathbf{y}_{cl}^T \mathbf{y}_{cl}}}{\sqrt{\mathbf{y}_{ol}^T \mathbf{y}_{ol}}}. \tag{30}$$

Substituting Eqs. 28 and 29 into 30 gives:

$$\frac{\|\mathbf{y}_{cl}(f)\|_2}{\|\mathbf{y}_{ol}(f)\|_2} = \frac{\sqrt{\mathbf{G}^T \mathbf{G}}}{\sqrt{\mathbf{G}^T \mathbf{G}}} S_i = S_i. \tag{31}$$

Therefore, for this special case of a single control input, a single disturbance input, and multiple output sensors, the input sensitivity is equal to the performance measure.

## References

[1] Shaw, L. L. and Shimovetz, R. M., "Weapons bay acoustic environment," AGARD-CP-549, Sept. 1994.

[2] Rockwell, D. and Naudascher, J., "Review: Self-sustaining oscillations of flow past cavities," *J. Fluids Eng.*, Vol. 100, 1978, pp. 152-165.

[3] Komerath, N. M., Ahuja, K. K., and Chambers, F. W., "Prediction and measurement of flows over cavities – a survey," AIAA Paper 87-0166, Jan. 1987.

[4] Chokani, N., "Flow induced oscillations in cavities – a critical survey," AIAA Paper 92-02-159, 1992.

[5] Rossiter, J. E., "Wind tunnel experiments on the flow over rectangular cavities at subsonic and transonic speeds," RAE Tech. Rep. 64037, Oct. 1964.

[6] Williams, D. R., Fabris, D., Iwanski, K., and Morrow, J., "Closed-loop control in cavities with unsteady bleed forcing," AIAA Paper 2000-0470, Jan. 2000.

[7] Williams, D. R., Fabris, D., and Morrow, J., "Experiments on controlling multiple acoustic modes in cavities," AIAA Paper 2000-1903, June 2000.

[8] Kegerise, M. A., Cattafesta, L. N., and Ha, C., "Adaptive identification and control of flow-induced cavity oscillations," AIAA Paper 2002–3158, June 2002.

[9] Cabell, R. H., Kegerise, M. A., Cox, D. E., and Gibbs, G. P., "Experimental feedback control of flow induced cavity tones," AIAA Paper 2002–2497, June 2002.

[10] Cattafesta, L. N., Garg, S., Choudhari, M., and Li, F., "Active control of flow-induced cavity resonance," AIAA Paper 1997–1804, June 1997.

[11] Williams, D. R. and Morrow, J., "Adaptive control of multiple acoustic modes in cavities," AIAA Paper 2001–2769, June 2001.

[12] Cattafesta, L. N., Shukla, D., Garg, S., and Ross, J. A., "Development of an adaptive weapons-bay suppression system," AIAA Paper 99–1901, June 1999.

[13] Cattafesta, L. N., Williams, D. R., Rowley, C. W., and Alvi, F. S., "Review of active control of flow-induced cavity resonance," AIAA Paper 2003–3567, June 2003.

[14] Cattafesta, L. N., Garg, S., Kegerise, M. A., and Jones, G.S., "Experiments on compressible flow-induced cavity oscillations," AIAA Paper 98–2912, June 1998.

[15] Kegerise, M. A., *An Experimental Investigation of Flow-Induced Cavity Oscillations*, PhD Thesis, Syracuse University, 1999.

[16] Kegerise, M. A., Spina, E. F., Garg, S., and Cattafesta, L. N., "Mode-switching and nonlinear effects in compressible flow over a cavity," *Physics of Fluids*, Vol. 16, No. 3, 2004, pp. 678-687.

[17] Astrom, K. J. and Wittenmark, B. , *Adaptive Control*, Addison-Wesley, Reading, MA, 1995.

[18] Juang, J., *Applied System Identification*, Prentice-Hall, Englewood Cliffs, NJ, 1994.

[19] Ljung, L., *System Identification: Theory for the User*, Prentice-Hall, Upper Saddle River, NJ, 1999.

[20] Juang, J., Horta, L. G., and Phan, M., "System/observer/controller identification toolbox," NASA TM–107566, Feb. 1992.

[21] Juang, J. and Phan, M., "Deadbeat predictive controllers," NASA TM–112862, May 1997.

[22] Juang, J. and Eure, K. W., "Predictive feedback and feedforward control for systems with unknown disturbances," NASA TM–1998–208744, Dec. 1998.

[23] Clarke, D. W., Mohtadi, C., and Tuffs, P. S., "Generalized predictive control – Part I. The basic algorithm," *Automatica*, Vol. 23, No. 2, 1987, pp. 137–148.

[24] Clarke, D. W., Mohtadi, C., and Tuffs, P. S., "Generalized predictive control – Part II. Extensions and interpretations," *Automatica*, Vol. 23, No. 2, 1987, pp. 149–160.

[25] Eure, K. W. and Juang, J., "Broadband noise control using predictive techniques," NASA TM–110320, Jan. 1997.

[26] Phan, M. Q., Lim, R. K., and Longman, R. W., "Unifying input-output and state-space perspectives of predictive control," MAE Tech. Report No. 3044, Princeton University, Princeton, NJ, 1998.

[27] Cattafesta, L. N., Garg, S., and Shukla, D., "Development of Piezoelectric Actuators for Active Flow Control," *AIAA Journal*, Vol. 39, No. 8, Aug. 2001, pp. 1562–1568.

[28] Mathew, J. , *A Theoretical and Experimental Study of Piezoelectric Unimorph Actuators for Active Flow Control*, M. S. Thesis, University of Florida, June 2002.

[29] Schaeffler, N. W., Hepner, T. E., Jones, G. S., and Kegerise, M. A., "Overview of active flow control actuator development at NASA Langley Research Center," AIAA Paper 2002-3159, June 2002.

[30] Heller, H. H., Holmes, D. G., and Covert, E. E., "Flow-induced pressure oscillations in shallow cavities," *J. Sound Vib.,* Vol. 18, No. 4, 1971, pp. 545–553.

[31] Rowley, C. W., Williams, D. R., Colonius, T., Murray, R. M., MacMartin, D. G., and Fabris, D., "Model-based control of cavity oscillations Part II: System identification and analysis," AIAA Paper 2002-0972, Jan. 2002.

[32] Rowley, C. W. and Williams, D. R., "Control of forced and self-sustained oscillations in the flow past a cavity," AIAA Paper 2003–0008, Jan. 2003.

[33] Williams, D. R., Rowley, C., Colonius, T., Murray, R., MacMartin, D., Fabris, D., and Albertson, J., "Model-based control of cavity oscillations Part I: Experiments," AIAA Paper 2002-0971, Jan. 2002.

[34] Hong, J. and Bernstein, D. S., "Bode integral constraints, colocation, and spillover in active noise and vibration control," *IEEE Trans. on Control Systems Tech.*, Vol. 6, No. 1, 1998, pp. 111–120.

[35] Franklin, G. F., Powell, J. D., and Workman, M. L., *Digital Control of Dynamic Systems*, Addison-Wesley, Menlo Park, CA, 1998.
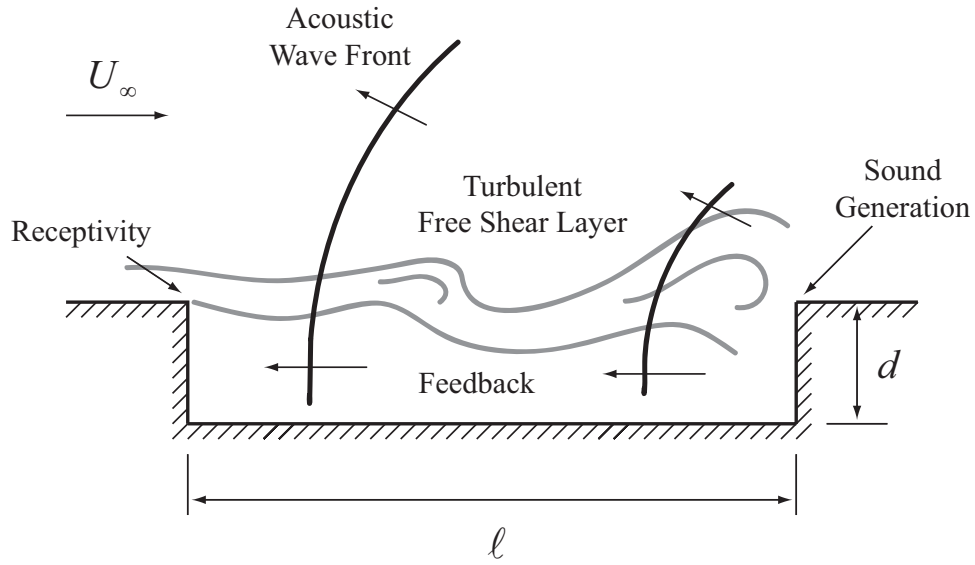
Fig. 1. Schematic illustrating the physical elements of flow-induced cavity tones.
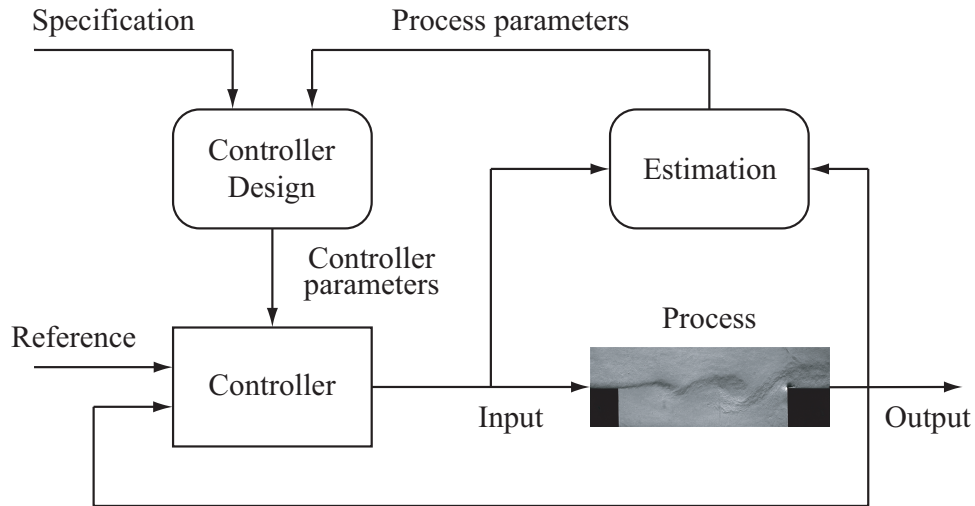


Fig. 2. Block diagram of a self-tuning adaptive controller (after Astrom and Wittenmark [17]).
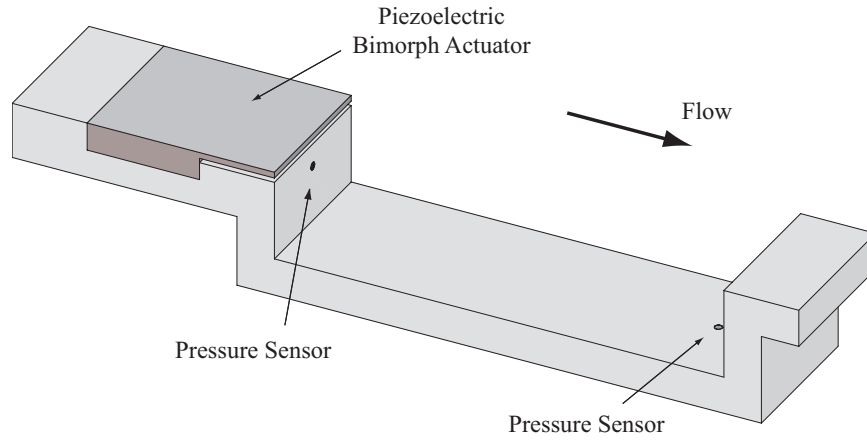
Fig. 3. Schematic of cavity model showing sensor and actuator locations.
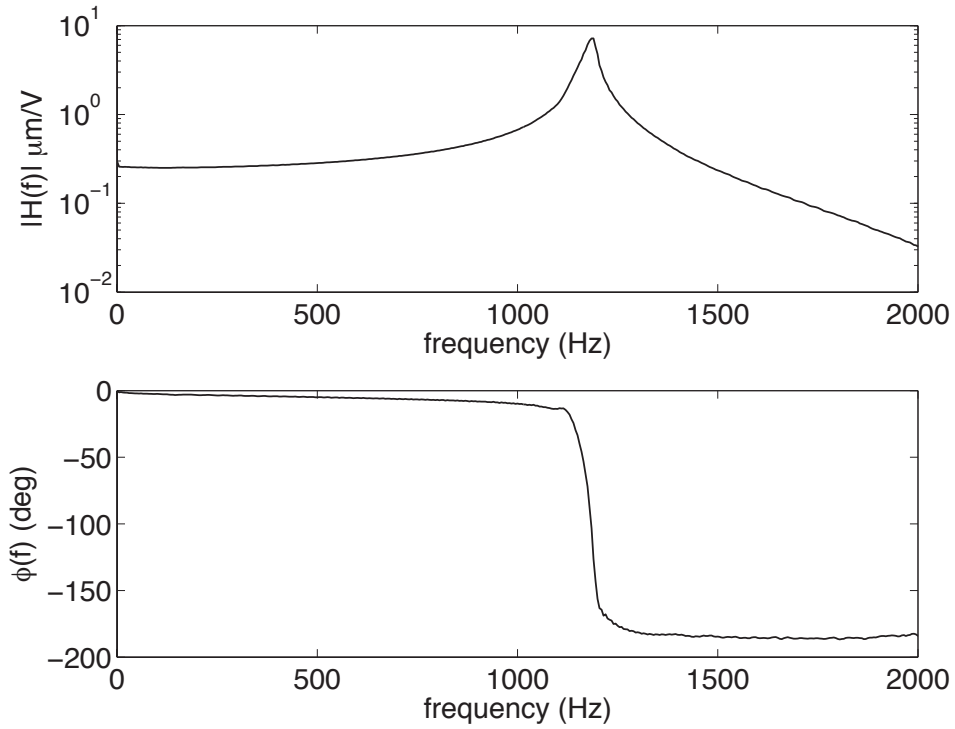


Fig. 4. Measured frequency response function from input voltage to output tip deflection of the bimorph actuator.
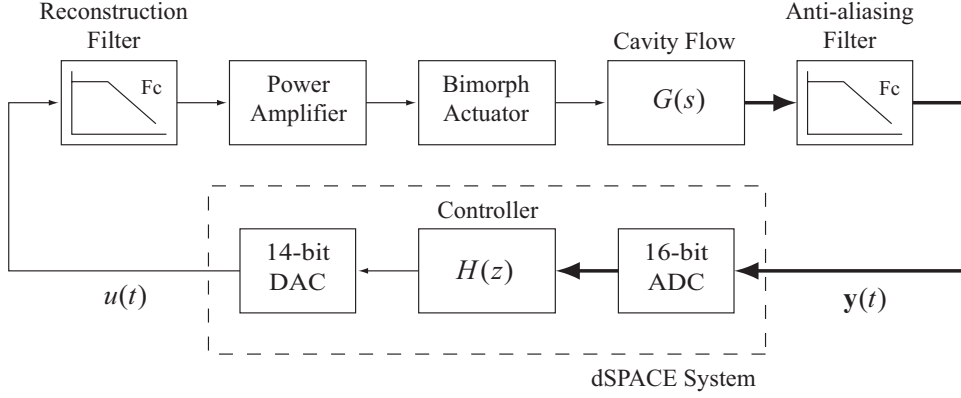
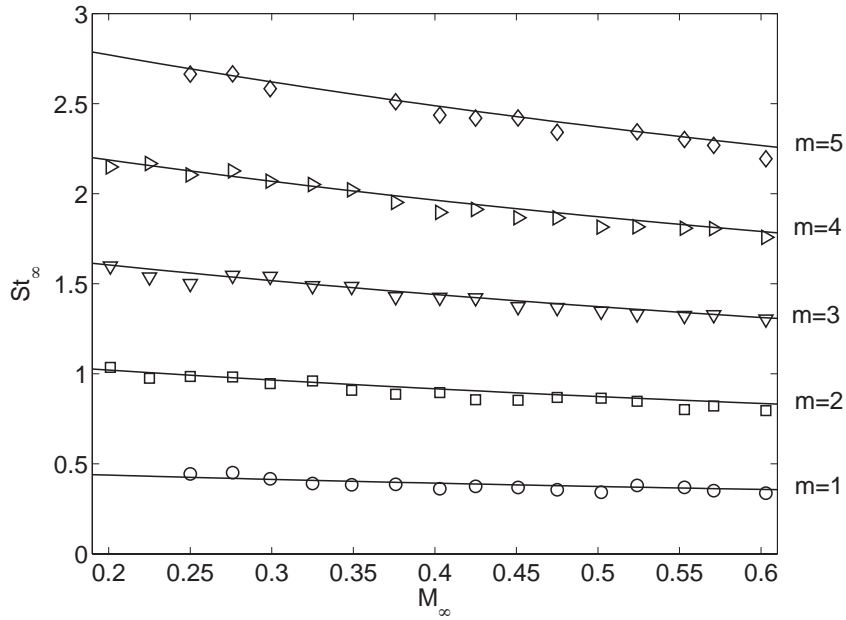Fig. 5. Block diagram of feedback control system.



Fig. 6. Acoustic response of $\ell/d = 5$ cavity. Symbols denote measured Rossiter-mode frequencies and solid lines denote the calculated Rossiter-mode frequencies.
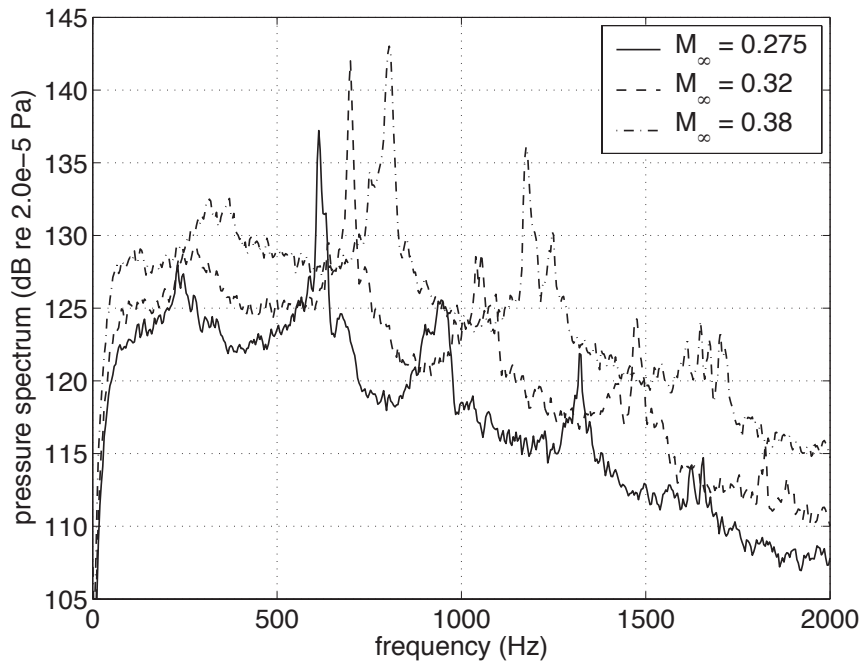
Fig. 7. Baseline pressure spectra of rear-floor sensor. $\ell/d = 5$.
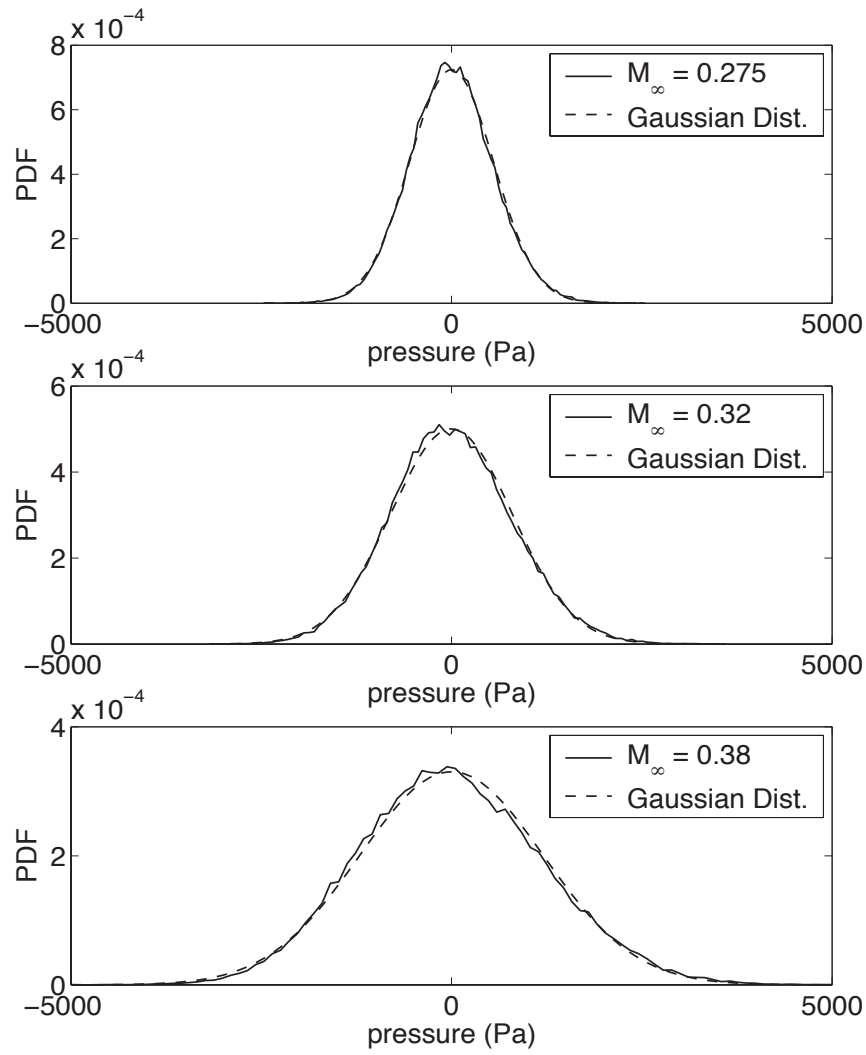
Fig. 8. Probability density functions of baseline rear-floor pressure for three Mach numbers.
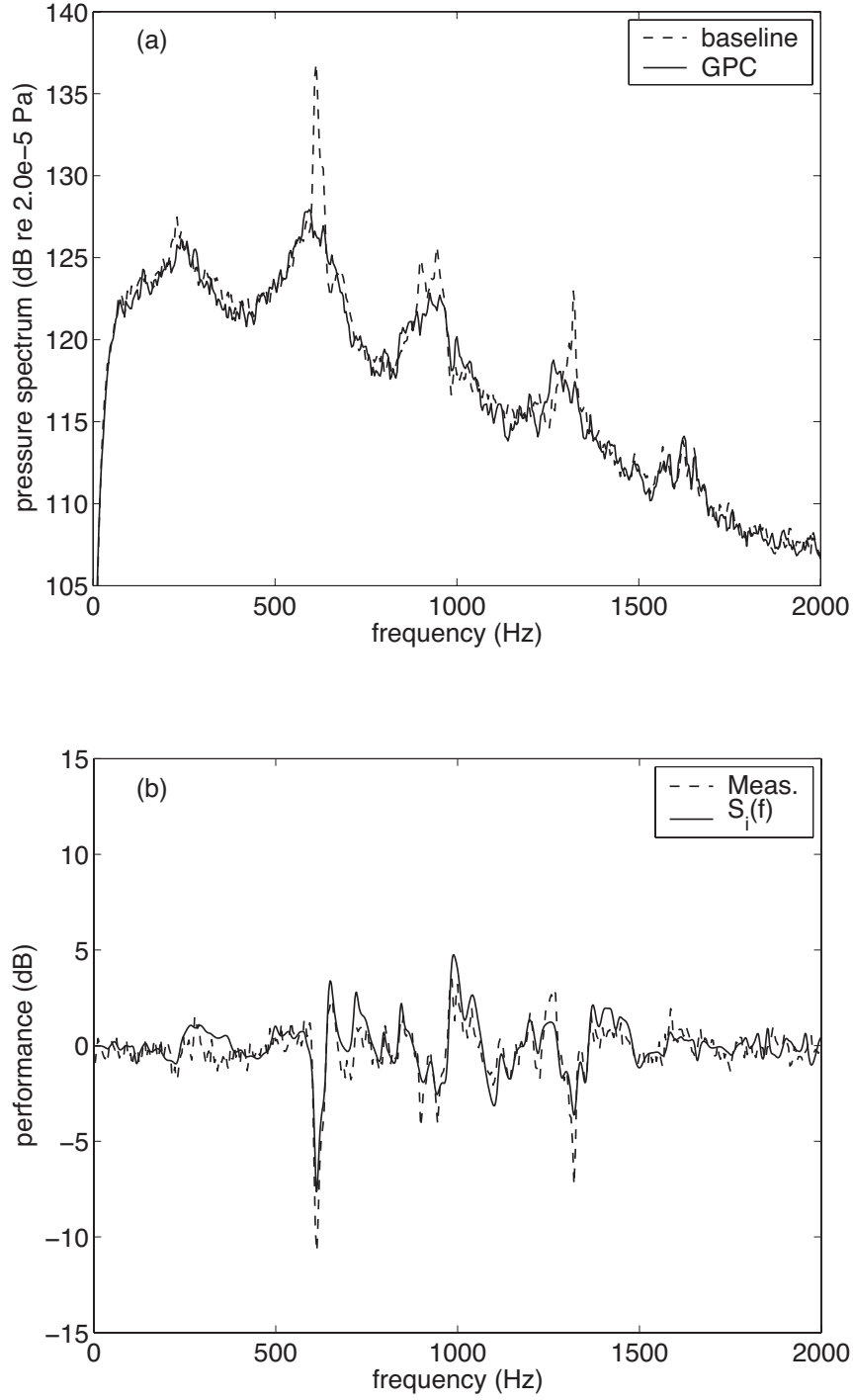
Fig. 9. GPC results at $M_\infty = 0.275$: a) baseline and controlled pressure spectra at rear-floor sensor, b) measured performance and input sensitivity.
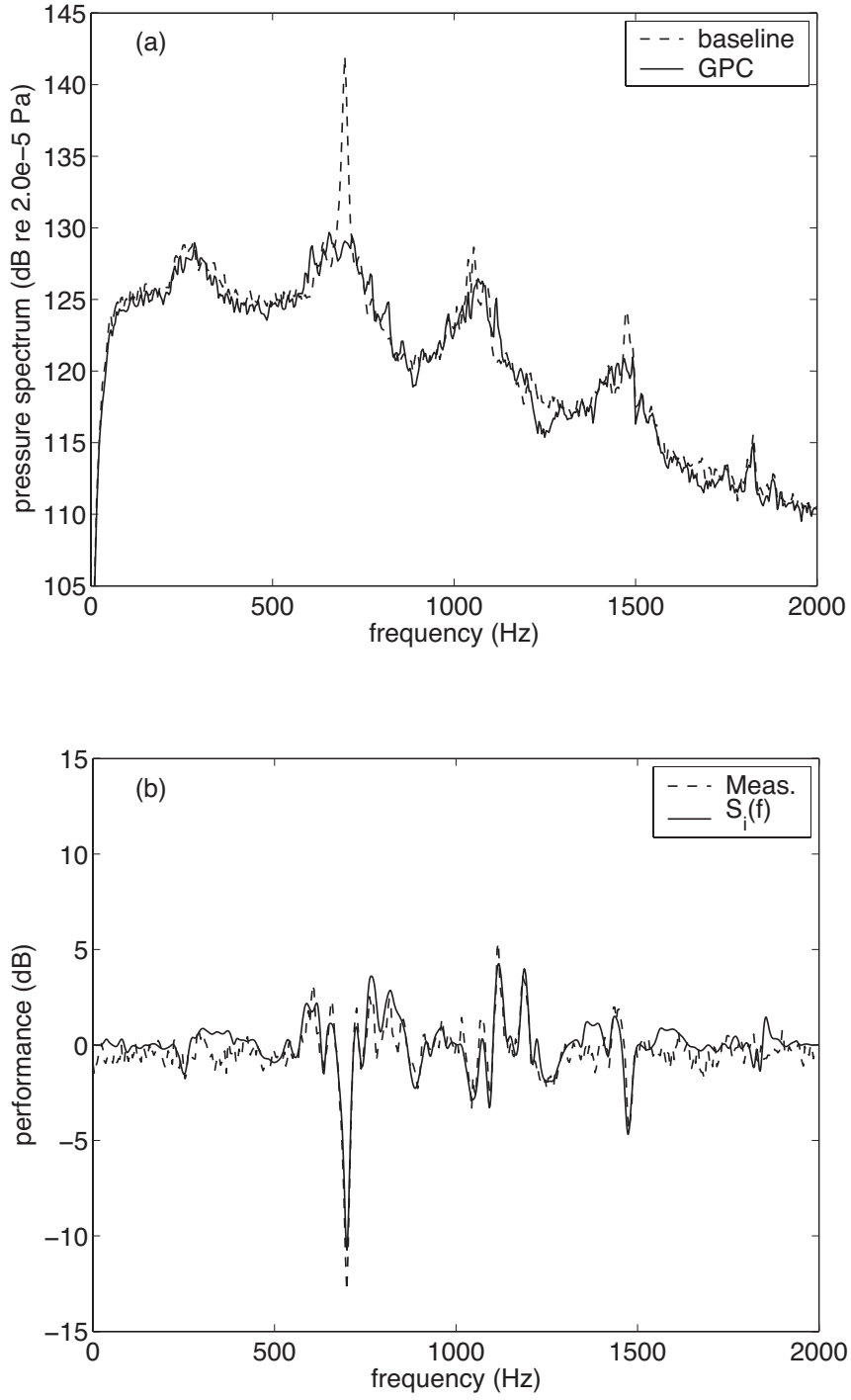
Fig. 10. GPC results at $M_\infty = 0.32$: a) baseline and controlled pressure spectra at rear-floor sensor, b) measured performance and input sensitivity.
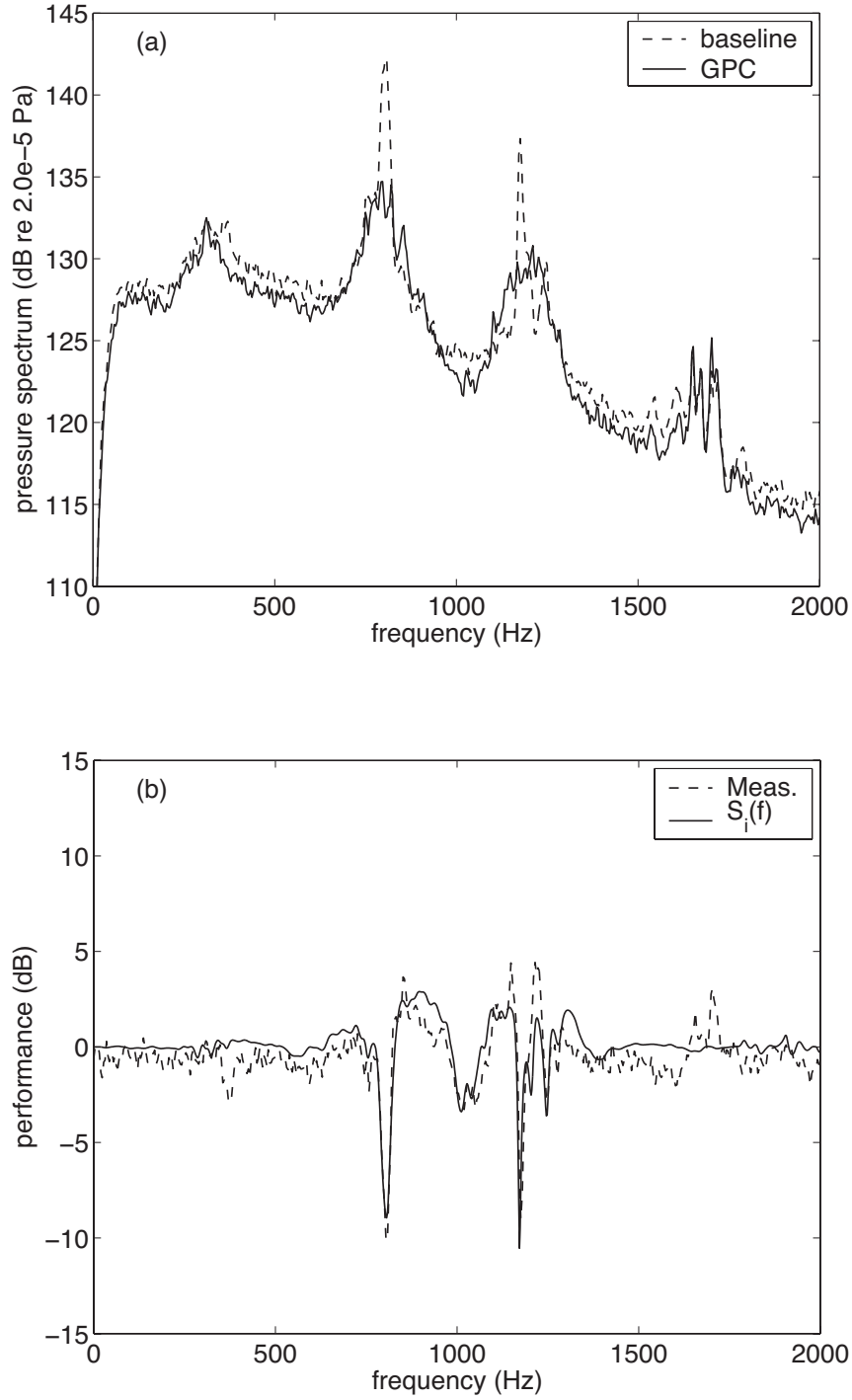
Fig. 11. GPC results at $M_\infty = 0.38$: a) baseline and controlled pressure spectra at rear-floor sensor, b) measured performance and input sensitivity.
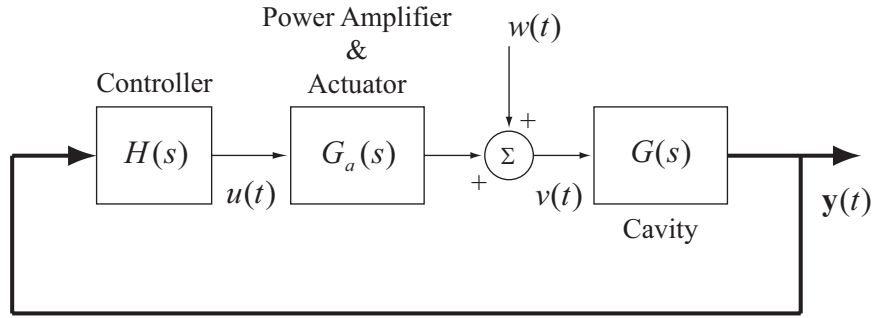
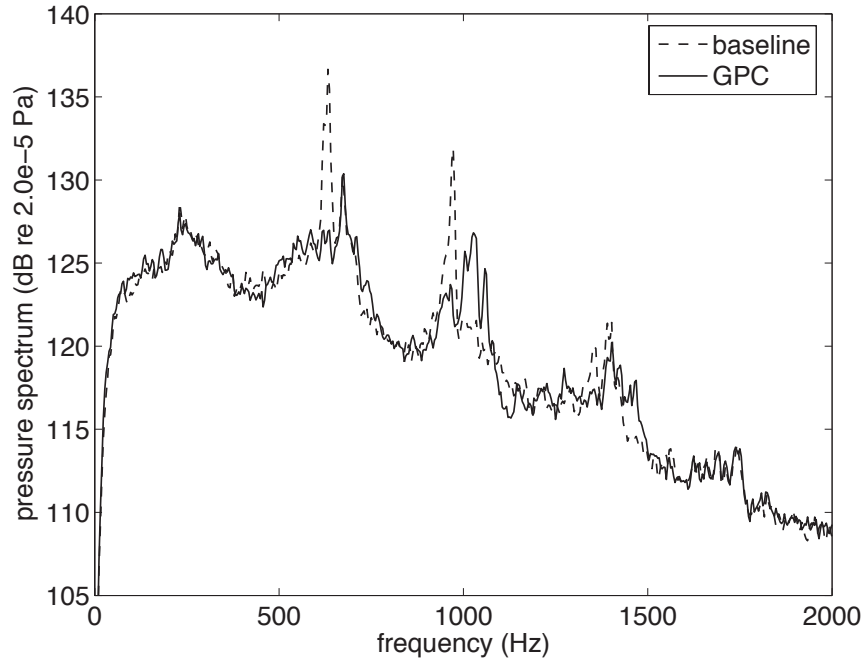Fig. 12. SIMO model of the cavity and controller.



Fig. 13. Baseline and controlled pressure spectra of rear-floor sensor. $M_\infty = 0.29$, $\ell/d = 5$.

Table 1: Measured vs. predicted frequencies (*Hz*) of the first 4 Rossiter modes

| | Mode 1 | | Mode 2 | | Mode 3 | | Mode 4 | |
|---|---|---|---|---|---|---|---|---|
| $M_\infty$ | Meas. | Pred. | Meas. | Pred. | Meas. | Pred. | Meas. | Pred. |
| 0.275 | 240 | 260 | 613 | 605 | 945 | 952 | 1320 | 1298 |
| 0.32 | 280 | 295 | 699 | 688 | 1054 | 1081 | 1475 | 1474 |
| 0.38 | 312 | 339 | 806 | 792 | 1175 | 1244 | 1650 | 1696 |

Table 2: GPC algorithm parameters

| | Model Order | Pred. Horizon | Sensor Weights | | Effort Penalty |
|---|---|---|---|---|---|
| $M_\infty$ | $p$ | $s$ | $q_1$ | $q_2$ | $\lambda$ |
| 0.275 | 80 | 240 | 0 | 1 | 0.05 |
| 0.32 | 80 | 240 | 0 | 1 | 0.10 |
| 0.38 | 80 | 240 | 0 | 1 | 0.25 |